# Supporting Information

# Mixed NiO/NiCo$_2$O$_4$ Nanocrystals Grown from Skeleton of 3D Porous Nickel Network as Efficient Electrocatalysts for Oxygen Evolution Reaction

*Chun Chang,[a,b] Lei Zhang,[a,c] Chan-Wei Hsu,[a] Xui-Fang Chuah,[a] and Shih-Yuan Lu[a*]*

*[a]Department of Chemical Engineering, National Tsing Hua University, Hsinchu 30013, Taiwan, Republic of China, E-mail: sylu@mx.nthu.edu.tw.*

*[b]College of Chemistry and Chemical Engineering, Bohai University, Jinzhou, Liaoning 121013, P.R. China.*

*[c]School of Materials Science and Engineering, Anhui University of Science and Technology, Huainan, Anhui 232001, P. R. China.*

**Development of criterion for *iR* compensation:**

For OER and HER study, the current densities achieved at specified applied potentials are the most important performance measurements. The current density vs. applied potential curve, the so-called polarization curve, is often recorded in a three electrode system. To correctly interpret the intrinsic electrocatalytic activity of the catalyst, the solution resistance, that causes extra potential bias interfering with the current density measurements, needs to be removed. This is the so-called *iR* compensation. It is crucial to conduct the *iR* compensation properly, otherwise the *iR*-compensated results are just misleading artifacts. This issue has been in general ignored and treated as a black box. Here, we developed a criterion for proper choice of the compensation level.

The basic idea is based on the following understanding. First, the solution resistance occurs mainly between the Luggin capillary of the reference electrode and the working electrode. This is particularly true for OER or HER, in which bubble evolution dominates the solution resistance. Second, the current density achieved depends on the distance between the Luggin capillary and the working electrode, higher current densities for shorter distances because of less solution resistances. Third, the *iR*-compensated current density would become irrelevant to the distance if the compensation level is proper. With the above understanding, one can determine a

proper compensation level for the specific OER or HER system based on polarization

curves recorded at increasing electrode distances, for which increasing compensation

levels are applied to obtain the corresponding $iR$-compensated polarization curves.

The highest compensation level, at which the $iR$-compensated polarization curves are

in reasonable agreement, serves to give proper $iR$ compensation.

Sample 20/20 was taken as an illustrating example. The relevant polarization

curves are presented in Fig. S1. Fig. S1(a) shows the polarization curves of sample

20/20 at three increasing electrode distances, 4, 8, and 12 mm. It is evident that the

current density increases with decreasing electrode distance as expected. The

corresponding $iR$-compensated polarization curves with increasing compensation

levels from 80, 85, 90, 95, to 100%, together with the un-compensated polarization

curves, are presented in Fig. S1(b)-S1(f), respectively. With compensation levels up to

90%, the three $iR$-compensated polarization curves are in reasonable agreement. With

compensation levels higher than 90%, the discrepancy between the three

$iR$-compensated polarization curves is significantly enlarged. The 90% compensation
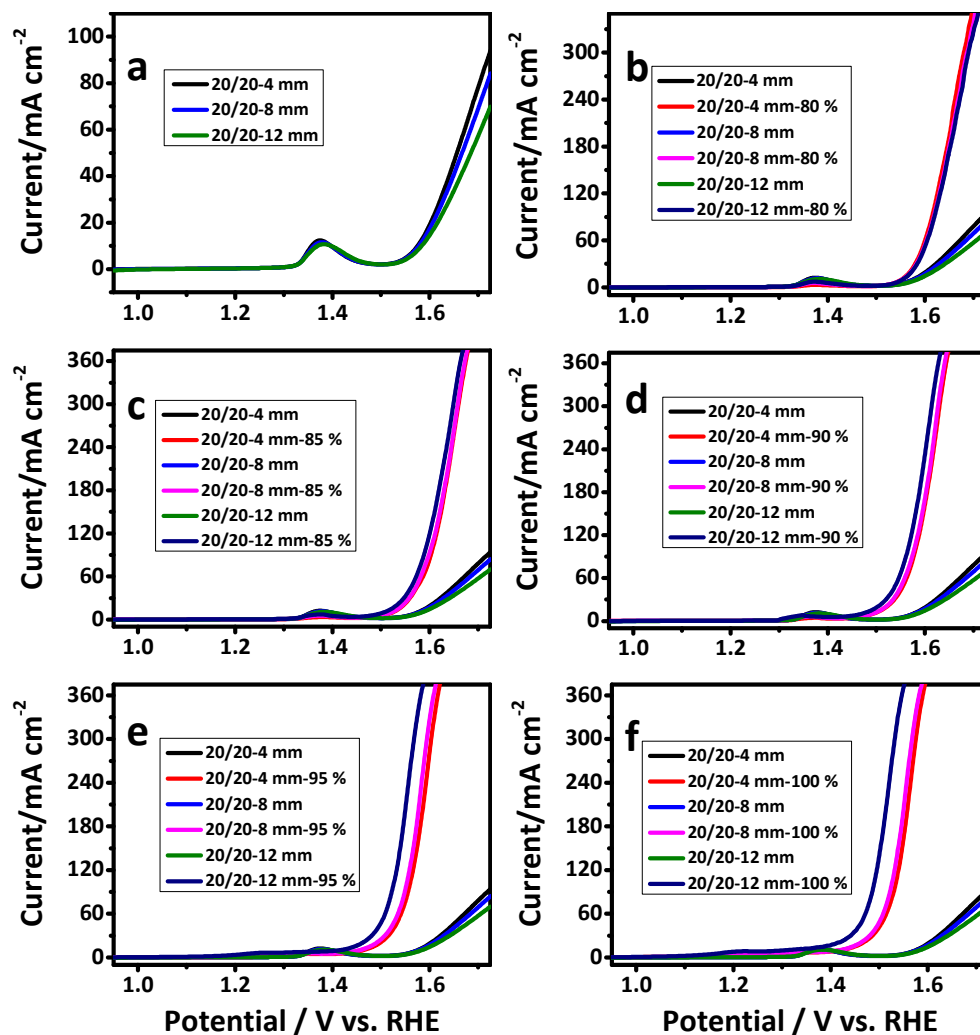
level was thus chosen for this case.

**Figure S1.** Polarization curves of sample 20/20: (a) un-compensated, (b) compensated at 80% level, (c) at 85%, (d) at 90%, (e) at 95%, and (f) at 100 %.
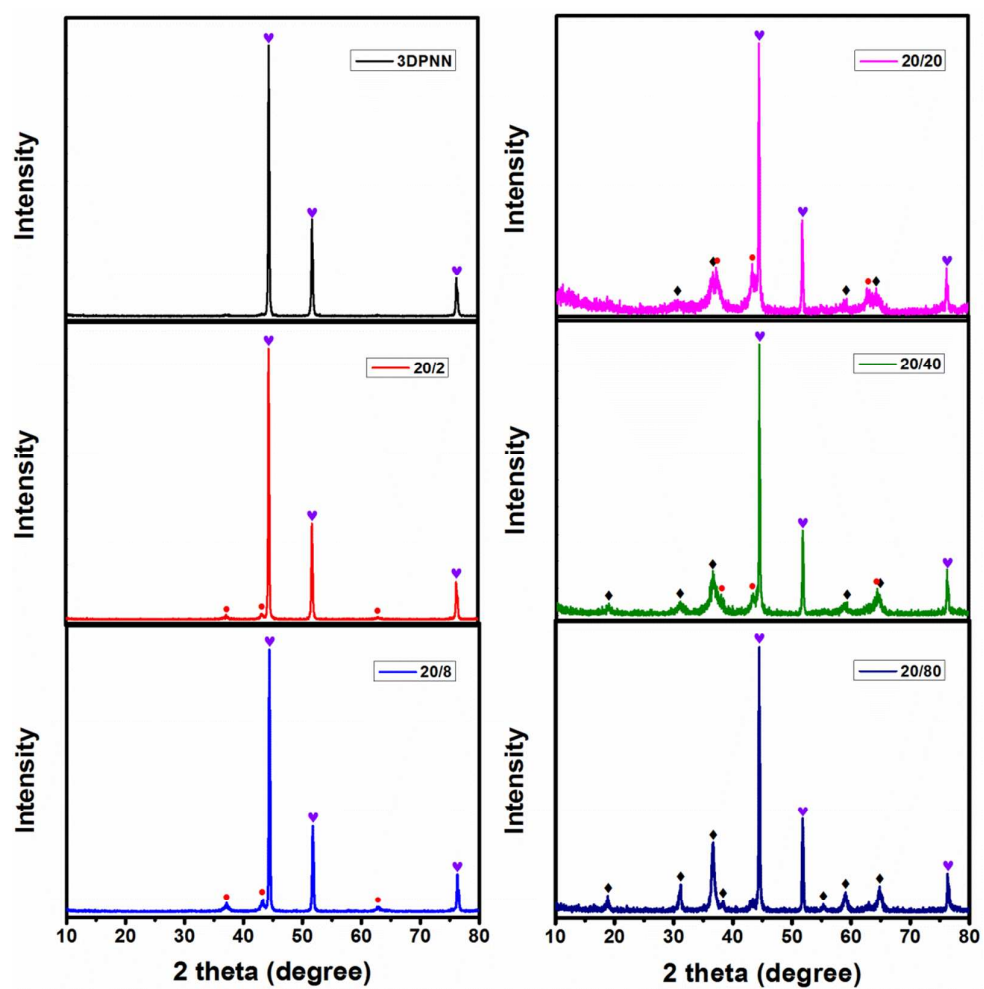
**Figure S2.** XRD patterns of 3DPNN and samples 20/2, 20/8, 20/20, 20/40, and 20/80.
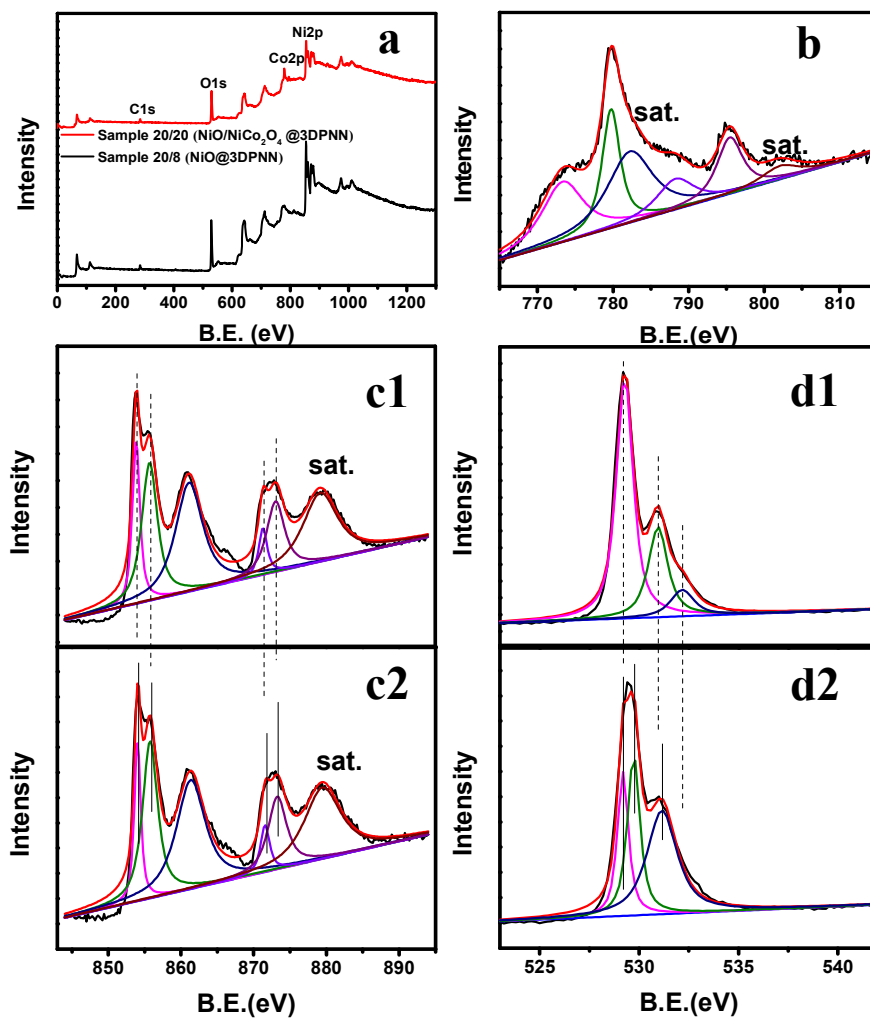
♥: Ni, ●NiO, ♦: $NiCo_2O_4$.

**Figure S3** XPS spectra of samples 20/8 and 20/20: (a) full survey spectra, (b) Co 2p of sample 20/20, (c1) Ni 2p of Ni sample 20/8, (c2) Ni 2p of sample 20/20, (d1) O 1s of sample 20/8, and (d2) O 1s of sample 20/20.
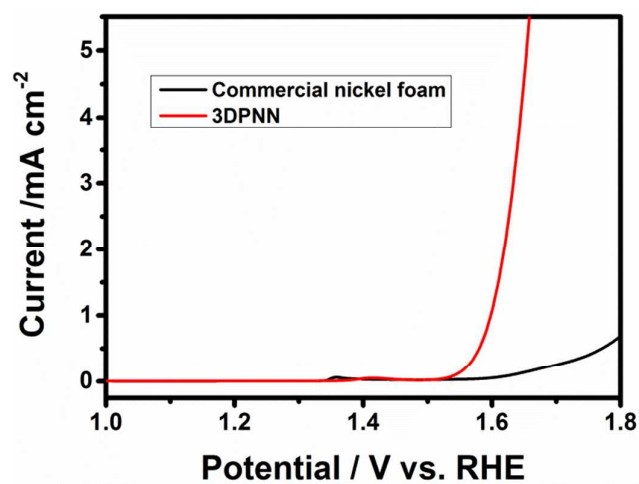
**Figure S4.** Polarization curves of commercial nickel foam and 3DPNN recorded in 1 M KOH at scan rate of 10 mV s$^{-1}$, with mass loading of electrocatalysts in working electrode controlled to be around 0.5 mg cm$^{-2}$.
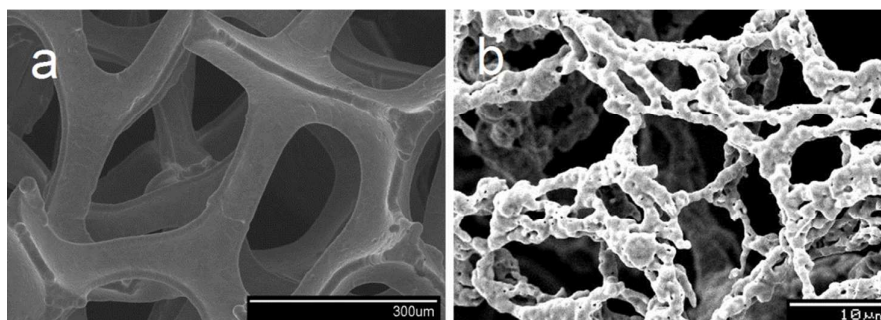
**Figure S5.** SEM images of (a) commercial Ni foam and (b) as-prepared 3D porous

nickel network (3DPNN). Note that scale bar for (a) is 300 μm and 10 μm for (b).
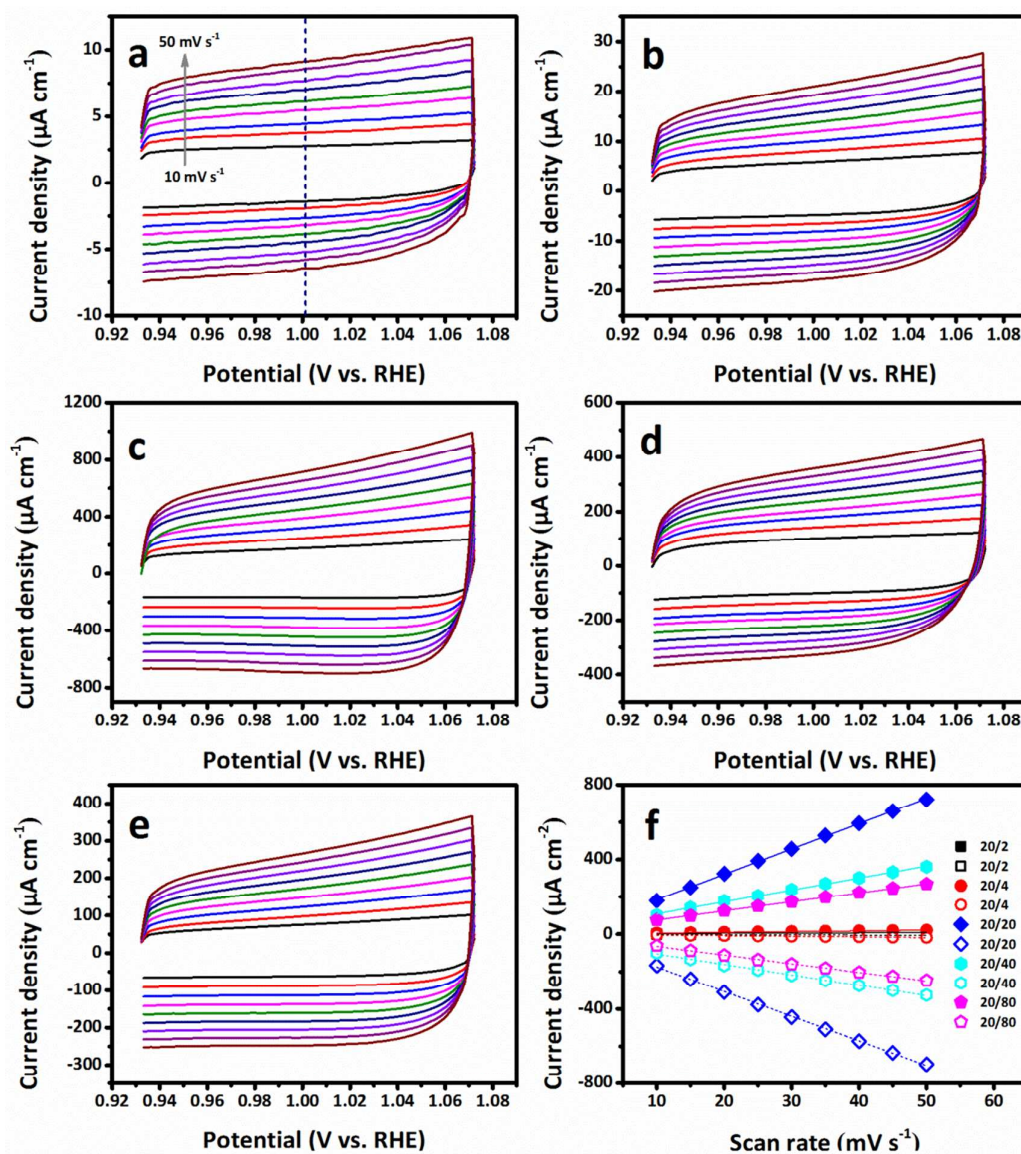
**Figure S6.** Cyclic voltammograms recorded at increasing scan rates in 1 M KOH: (a) 20/2, (b) 20/4, (c) 20/20, (d) 20/40, (e) 20/80. (f) Linear fitting of capacitive current density achieved at 1.0022 V vs. RHE *vs.* scan rate in 1.0 M KOH.
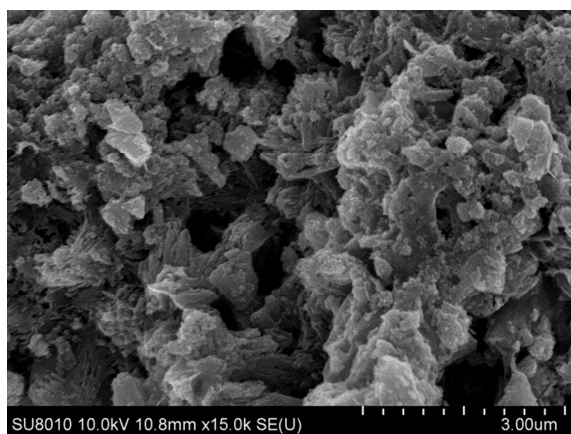
**Figure S7.** SEM image of NiO/NiCo$_2$O$_4$@3DPNN electrocatalyst after 12 h OER

operation.

**Table S1**. Comparison of OER performances: present work *vs*. literature.

| Catalyst | $\eta_{10}$/mV | Mass activity ($\eta$=350 mA)/A g$^{-1}$ | Tafel slope/mV dec$^{-1}$ | Reference |
|---|---|---|---|---|
| NiCo$_2$O$_4$/NiO@3D porous nickel network | 263 ($\eta_{100}$= 350) ($\eta_{250}$= 389) | 200 | 79 | This work |
| NiO/Ni foam | 345 | — | 53 | [1] |
| porous Co$_3$O$_4$ nanosheets | 368 | — | 59 | [2] |
| Ni-Co oxide hierarchical nanosheets | 340 | — | 51 | [3] |
| Co$_3$O$_4$ | 377 | — | 58 | [4] |
| mesoporous Co$_3$O$_4$ nanoflakes | 380 | — | 48 | [5] |
| iron-cobalt oxide nanosheets | 308 | 54.9 | 36.8 | [6] |
| cobalt-nickel hydroxide nanosheets on Ni foam | 366 | — | 72 | [7] |
| NiCo$_2$O$_4$ nanocage | 340 | — | 75 | [8] |
| Nickel cobalt oxide hollow nanosponges | 362 | — | 64 | [9] |
| Nickel-cobalt layered double hydroxide nanosheets | 419 | 30.6 ($\eta$=700 mV) | 113 | [10] |
| porous NiCo$_2$O$_4$ nanosheets | 379 | — | 63.4 | [11] |
| Ni$_3$Se$_2$-Au@glass (annealed) | 290 | — | 97.2 | [12] |
| CoP$_3$ Nano-needle Array/CFP | 334 ($\eta_{50}$= 407) | — | 62 | [13] |
| Zn/Co hydroxy sulfate | 370 | 146 ($\eta$=370 mV) | 60 | [14] |

**Video S1.** Showing oxygen evolution at 250 mA/cm$^2$ (MP4).

**SI REFERENCES**

(1) Liang, J.; Wang, Y.-Z.; Wang, C.-C.; Lu, S.-Y. In Situ Formation of NiO on Ni Foam Prepared with a Novel Leaven Dough Method as an Outstanding Electrocatalyst for Oxygen Evolution Reactions. *Journal of Materials Chemistry A* **2016,** *4*, 9797-9806.

(2) Li, Z.; Yu, X.-Y.; Paik, U. Facile Preparation of Porous $Co_3O_4$ Nanosheets for High-Performance Lithium Ion Batteries and Oxygen Evolution Reaction. *Journal of Power Sources* **2016,** *310*, 41-46.

(3) Wang, H. Y.; Hsu, Y. Y.; Chen, R.; Chan, T. S.; Chen, H. M.; Liu, B. $Ni^{3+}$-Induced Formation of Active NiOOH on the Spinel Ni‒Co Oxide Surface for Efficient Oxygen Evolution Reaction. *Advanced Energy Materials* **2015,** *5*, 1500091.

(4) Jeon, H. S.; Jee, M. S.; Kim, H.; Ahn, S. J.; Hwang, Y. J.; Min, B. K. Simple Chemical Solution Deposition of $Co_3O_4$ Thin Film Electrocatalyst for Oxygen Evolution Reaction. *ACS Applied Materials & Interfaces* **2015,** *7*, 24550-24555.

(5) Chen, S.; Zhao, Y.; Sun, B.; Ao, Z.; Xie, X.; Wei, Y.; Wang, G. Microwave-Assisted Synthesis of Mesoporous $Co_3O_4$ Nanoflakes for Applications in Lithium Ion Batteries and Oxygen Evolution Reactions. *ACS Applied Materials & Interfaces* **2015,** *7*, 3306-3313.

(6) Zhuang, L. H.; Ge, L.; Yang, Y. S.; Li, M. R.; Jia, Y.; Yao, X. D.; Zhu, Z. H. Ultrathin Iron-Cobalt Oxide Nanosheets with Abundant Oxygen Vacancies for the Oxygen Evolution Reaction. *Advanced Materials* **2017,** *29*, 1606793.

(7) Liu, X.; Xu, D.; Zhang, D.; Zhang, G.; Zhang, L. Superior Performance of 3 D Co-Ni Bimetallic Oxides for Catalytic Degradation of Organic Dye: Investigation on the Effect of Catalyst Morphology and Catalytic Mechanism. *Applied Catalysis B: Environmental* **2016,** *186*, 193-203.

(8) Lv, X.; Zhu, Y.; Jiang, H.; Yang, X.; Liu, Y.; Su, Y.; Huang, J.; Yao, Y.; Li, C. Hollow Mesoporous $NiCo_2O_4$ Nanocages as Efficient Electrocatalysts for Oxygen Evolution Reaction. *Dalton Transactions* **2015,** *44*, 4148-4154.

(9) Zhu, C.; Wen, D.; Leubner, S.; Oschatz, M.; Liu, W.; Holzschuh, M.; Simon, F.; Kaskel, S.; Eychmuller, A. Nickel Cobalt Oxide Hollow Nanosponges as Advanced Electrocatalysts for the

Oxygen Evolution Reaction. *Chemical Communications* **2015,** *51*, 7851-7854.

(10) Jiang, J.; Zhang, A.; Li, L.; Ai, L. Nickel–Cobalt Layered Double Hydroxide Nanosheets as High-Performance Electrocatalyst for Oxygen Evolution Reaction. *Journal of Power Sources* **2015,** *278*, 445-451.

(11) Zhu, Y. L.; Zhou, W.; Yu, J.; Chen, Y. B.; Liu, M. L.; Shao, Z. P. Enhancing Electrocatalytic Activity of Perovskite Oxides by Tuning Cation Deficiency for Oxygen Reduction and Evolution Reactions. *Chemistry of Materials* **2016,** *28*, 1691-1697.

(12) Swesi, A. T.; Masud, J.; Nath, M. Nickel Selenide as a High-Efficiency Catalyst for Oxygen Evolution Reaction. *Energy & Environmental Science* **2016,** *9*, 1771-1782.

(13) Wu, T.; Pi, M.; Zhang, D.; Chen, S. 3D Structured Porous $CoP_3$ Nanoneedle Arrays as an Efficient Bifunctional Electrocatalyst for the Evolution Reaction of Hydrogen and Oxygen. *Journal of Materials Chemistry A* **2016,** *4*, 14539-14544.

(14) Dutta, S.; Ray, C.; Negishi, Y.; Pal, T. Facile Synthesis of Unique Hexagonal Nanoplates of Zn/Co Hydroxy Sulfate for Efficient Electrocatalytic Oxygen Evolution Reaction. *ACS Applied Materials & Interfaces* **2017,** *9*, 8134-8141.